Journal of Molecular Liquids 377 (2023) 121559

Contents lists available at ScienceDirect

Journal of Molecular Liquids

journal homepage: www.elsevier.com/locate/molliq

Adsorption of 40 low molecular weight drugs on pristine and fluorinated C_{60} fullerenes: *Ab initio*, statistical and neural networks analysis

Elizaveta B. Kalika [a,b], Nikolay V. Bondarev [c], Konstantin P. Katin [a,d,*], Alexey I. Kochaev [a,e], Anastasiya A. Grekova [d], Savas Kaya [f], Yusupbek A. Bauetdinov [d], Mikhail M. Maslov [a,d]

[a] Laboratory of Computational Design of Nanostructures, Nanodevices, and Nanotechnologies, Research Institute for the Development of Scientific and Educational Potential of Youth, Aviatorov str. 14/55, Moscow 119620, Russia
[b] Moscow Institute of Physics and Technology (National Research University), 1A Kerchenskaya st., Moscow 117303, Russia
[c] Department of Physical Chemistry, V. N. Karazin Kharkiv National University, 4 Svobody Sq., 61022 Kharkiv, Ukraine
[d] Department of Condensed Matter Physics, National Research Nuclear University "MEPhI", Kashirskoe Sh. 31, 115409 Moscow, Russia
[e] Research and Education Center "Silicon and Carbon Nanotechnologies", Ulyanovsk State University, 42 Leo Tolstoy Str., 432017 Ulyanovsk, Russia
[f] Department of Chemistry, Faculty of Science, Sivas Cumhuriyet University, 58140 Sivas, Turkey

ARTICLE INFO

Article history:
Received 23 November 2022
Revised 13 February 2023
Accepted 27 February 2023
Available online 5 March 2023

Keywords:
Drug delivery
Drug carrier
Density functional theory
C_{60} fullerene
Adsorption energy

ABSTRACT

Loading of 40 small drugs molecules with molecular weights in 47–210 g/mol range consisted of H, C, N, O, F, S elements on C_{60}, $C_{60}F_2$ and $C_{60}F_{48}$ fullerenes are studied with the density functional theory. Adsorption energies as well as deformation energies of fullerenes and drugs are calculated. The $C_{60}F_2$ is recognized as the most active drugs adsorbent. Mean adsorption energies averaged over all considered drugs are 0.41, 0.59 and 0.54 eV with standard deviations of 0.10, 0.09 and 0.14 eV for C_{60}, $C_{60}F_2$ and $C_{60}F_{48}$ fullerenes, respectively. Mean energies of drug-induced deformations of C_{60}, $C_{60}F_2$ and $C_{60}F_{48}$ are 8.6, 12.0 and 16.6 meV, respectively. Multilinear regressions and neural networks were proposed for prediction of adsorption energies based on dipole moments and frontier molecular orbitals of the drugs. Achievable accuracy of such predictions is about 0.1 eV. Altretamine antibiotic is recognized as the notable drug possessing extremely high binding energies about 1 eV with fullerenes. Infrared spectral shifts due to its loading on fullerene carriers are calculated.

1. Introduction

Carbon fullerene C_{60} is regarded as a promise basis for drugs carrier systems. This fullerene is a stable bio comparable nanoparticle with well-defined structure and suitable diameter of about 0.7 nm. It is non-toxic and even has a positive effect on human health [1]. The presence of sp^2-hybridized carbon atoms provides wide opportunities for functionalization and thus tuning the solubility of the fullerene. The stable skeleton is suitable for embedding of heteroatoms, which act as adsorption centers and provide reliable adhesion to small molecules. In recent years, researchers have examined the interaction of C_{60} fullerene and its derivatives with dozens of drugs. *In vitro* experiments confirmed that some anticancer drugs loaded on C_{60} are much more efficient compared to the same drugs disconnected from the fullerene [2]. Muz *et.al* concluded that BN-doped fullerene is a suitable carrier for favipiravir, a widely used anti-COVID medicament [3]. Esrafili and Khan reported that alkali metals doped C_{60} possesses moderate interaction with popular anticancer drug 5-fluorouracil, and assumed its appropriate releasing due to protonation inside the tumor [4]. Fouejio *et.al* found the pristine C_{60} to be suitable for delivery of dihydroartemisinin and improving its suitability [5]. Parlak *et.al* proposed Si-doped C_{60} for delivery of nolnupiravir and for detecting this antivirus drug at water environment [6]. Wang *et.al* recognized Si, B and Al-doped C_{60} as promising carriers for hydroxyurea delivery [7]. Neal *et.al* reported enhancing the polarity of C_{60} due to loading of some anticancer antibiotics [8]. Nouraliei *et.al* considered C_{60} as well as smaller C_{30} and larger C_{90} fullerenes as the carriers of phenelzine and ins derivatives [9]. Many other studies were dedicated to interaction of C_{60} with different drugs, including 6-mercaptopurine [10], curcumin [11], endophytic fungus [12], fluoroquinolone antibiotic [13], oxadiazole [14] and amphetamine [15].

Fluorinated fullerenes are of particular interest for drug delivery applications. Attention to them is explained by the advantages of fluorine, which have recently been demonstrated by the example of fluorinated graphene. Involving of fluorine into delivery system

* Corresponding author.
E-mail address: KPKatin@yandex.ru (K.P. Katin).

https://doi.org/10.1016/j.molliq.2023.121559
0167-7322/

provides its high near infrared absorbance and the possibility of effective photothermal therapy, as well as better drugs loading due to strong non-covalent interaction [16,17]. Ultra-small soluble flakes of fluorinated graphene demonstrates switchable fluorescence as well as controlled and pH-responsive drugs release [17]. Highly fluorinated graphene oxide prepared from ionic liquid exhibited very high curcumin-loading efficiency to deliver anticancer drugs [18]. Moreover, such carriers provide high magnetic resonance imaging contrast sufficient for the *in vivo* control of the delivery process [19]. Based on their experimental and theoretical studies, Gong *et.al* noted "excellent photothermal performance in the near infrared region, a high drug loading capacity, pH-triggered drug release, low cytotoxicity and good combination therapy effects" of fluorinated graphene [20]. Additional advantage of drugs carriers based on fluorinated graphene is their experimentally demonstrated turn-off fluorescence properties [21,22]. In contrast to graphene flakes, fluorinated C_{60} fullerenes possess well-defined structure, uniform size [23] and better adsorption due to higher curvature [11,24]. In previous studies, fluorinated C_{60} were examined as the carriers of some anticancer [23] and anti-COVID drugs [25].

In all the mentioned studies, the authors considered a single or only a few practically interesting drugs loaded on fullerene, without extensive comparison with other drugs. In this article, we aimed to investigate systematically the interaction of fullerene with drugs. Therefore, we considered a set of 40 common low-molecular-weight drugs loaded on the pristine and fluorinated C_{60}s. Consideration of a large number of drugs provides some statistical conclusions and determination of the typical behavior of drugs on the fullerene surface.

2. Meterials and Methods

Geometry optimizing of all drugs, fullerenes and their complexes was performed with GPU-accelerated TeraChem software [26] combined with efficient geomeTRIC optimizer [27]. The lowest energies adsorption positions were selected by the algorithm described in our previous work [23]. The values of E_b, E_{def}(full) and E_{def}(drug) were calculated as it is described in the same Ref. [23]. The B3LYP/6-31G** level of theory [28,29,30] was applied to both optimizing and infrared frequencies calculations. Since we considered only energy minima (not transition states), all frequencies are real. Corrections for basis set superposition errors and dispersion interactions [31] were included. Statistical and neural networks analysis was performed according with the protocol described in Ref. [32] using STATISTICA program package [33] Atomistic structures were visualized with the VESTA software [34].

The pristine C_{60} was considered along with two fluorinated derivatives, $C_{60}F_2$ and $C_{60}F_{48}$, shown in Fig. 1. Fullerenes with exactly this amount of fluorine are the most stable and represent realistic models of low- and high-fluorinated cages (for a detailed discussion of their stability, see our previous study [23]). The most stable configuration of carbon skeleton with I_h symmetry was adopted. The lowest energy isomers were considered for fluorinated fullerenes $C_{60}F_2$ and $C_{60}F_{48}$ [23]. We investigated the non-covalent loading of drugs on these fullerenes. A set of 40 drugs with the lowest molecular weights was taken from the DrugBank database [35]. We limited ourselves to metal-free drugs molecules composed of common chemical elements C, H, N, O, S, F. Their names and formulas are listed in Table 1, whereas structures are shown in Supplementary materials Figure S1.

For each drug, we considered different loading positions and found the strongest adsorption energy with the density functional theory, as described in Ref. [23]. Interaction between fullerene and drug was quantitatively characterized by binding energy E_b and deformation energies of fullerene E_{def}(full) and drug E_{def}(drug), respectively. We also calculated frontier molecular orbitals HOMO and LUMO and dipole moments D of pristine and loaded drugs. According to conceptual density functional theory, these values can define chemical activity of molecules and therefore influence on the interaction energies. Full set of calculated data for drugs loaded on C_{60}, $C_{60}F_2$ and $C_{60}F_{48}$ fullerenes is presented in supplementary materials Tables S1, S2 and S3, respectively.

3. Results and discussion

3.1. Effect of fluorination on interaction between C_{60} and drugs

Table 2 shows the ranges of E_b, E_{def}(full) and E_{def}(drug) values as well as arithmetic means and standard deviations of these energies. According to the data presented, low-fluorinated fullerene $C_{60}F_2$ possesses the strongest interaction with drugs. Previously, similar behavior was reported for doxorubicin anticancer drug [23]. This can be explained by the fact that both the fluorinated and non-fluorinated parts of the fullerene surface are available for the drug. One can also see from Table 2, that fluorinated cages with movable C–F bonds provide more opportunities for fullerenes deformation. However, drugs are on average more deformed because of interaction, since they are less rigid.

3.2. Statistical correlations

Pair correlations coefficients for the values of the binding energy E_b, deformation energies E_{def}(full) and E_{def}(drug), as well

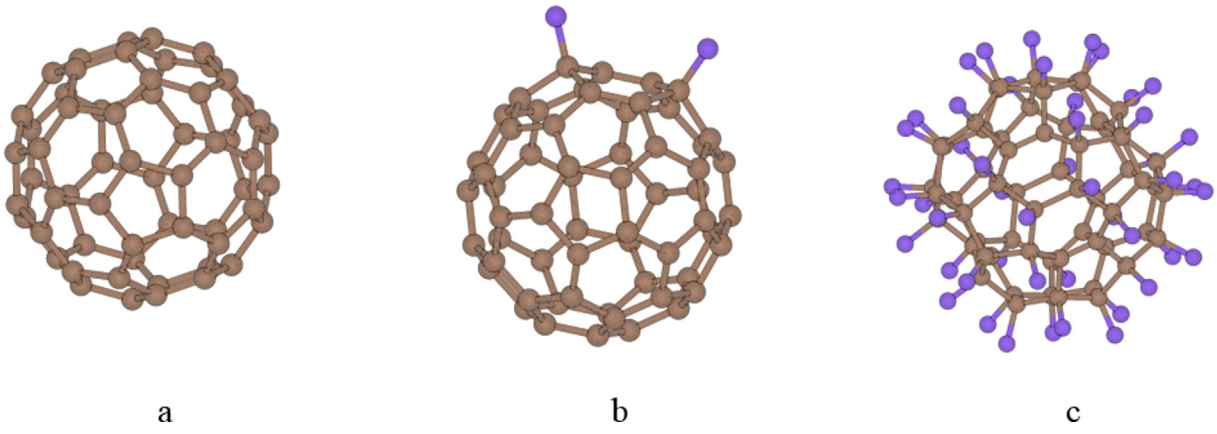

Fig. 1. Atomistic models of pristine C_{60} (a) and its $C_{60}F_2$ (b) and $C_{60}F_{48}$ (c) fluorinated derivatives. The brown and purple balls represent carbon and fluorine atoms, respectively. (For interpretation of the references to colour in this figure legend, the reader is referred to the web version of this article.)

as frontier orbitals HOMO and LUMO and dipole moments D of the pristine and loaded on fullerenes drugs are presented in Table 3. According to Chaddock scale, the coefficients values higher than 0.5 indicate a significant correlation. One can see that the HOMO of pristine drug correlates positively with HOMO of C_{60} + drug complex. This indicates that the drug significantly contributes to HOMO of the complex. Note that the HOMOs of C_{60} and $C_{60}F_2$ has a moderate values (−5.90 and −5.94 eV, respectively), which are close to typical HOMOs of the most drugs. The $C_{60}F_{48}$ has a very deep lying HOMO (−9.70 eV). Therefore, the HOMO of the "$C_{60}F_{48}$ + drug" complexes are localized mostly on drugs and strongly correlate with the HOMOs of pristine drug. This fact is indicated by very high value of corresponding correlation coefficient (it equals to 0.972, see Table 3). In addition, dipole moments of the complexes correlate with those of pristine drugs. This is because the C_{60} and $C_{60}F_{48}$ have not their own dipole moments, and $C_{60}F_2$ has moderate own moment (2.28 Debye).

It is a remarkable fact that E_b does not correlate with other considered values. As widely assumed, frontier orbitals and dipole moments of drugs defines their global reactivity. However, none of them possessed any statistical correlation with E_b. To further analyze relationship between E_b and other values, we derived a multiple linear regressions for E_b (see Table 4). We obtained multiple coefficient of determination R^2 in 0.15–0.5 range, which indicates a low predictive power of these regressions. Maximal, minimal and mean absolute differences between actual and predicted values of E_b are collected in Table 4. They provides estimation of accuracy of the E_b prediction with multiple linear regressions.

Table 1
Names, chemical formulas and molecular weights of 40 considered drugs.

#	Name	Formula	Molecular weight, g/mol
1	Methoxyamine	CH_5NO	47.057
2	Dacarbazine	$C_6H_{10}N_6O$	182.18
3	Amifampridine	$C_5H_7N_3$	109.13
4	Altretamine	$C_9H_{18}N_6$	210.28
5	Pimagedine	CH_6N_4	74.09
6	Cysteamine	C_2H_7NS	77.15
7	Sarcosine	$C_3H_7NO_2$	89.09
8	Thiotepa	$C_6H_{12}N$	189.22
9	Biguanide	$C_2H_7N_5$	101.11
10	gamma-Aminobutyric acid (GABA)	$C_4H_9NO_2$	103.12
11	Imexon	$C_4H_5N_3O$	111.10
12	Histamine	$C_5H_9N_3$	111.15
13	Creatinine	$C_4H_7N_3O$	113.12
14	Thiosulfic acid	$H_2O_3S_2$	114.15
15	Muscimol	$C_4H_6N_2O_2$	114.10
16	Ethyl pyruvate	$C_5H_8O_3$	116.11
17	2,4-thiazolidinedione	$C_3H_3NO_2S$	117.13
18	Niacin	$C_6H_5NO_2$	123.11
19	Pyrazinamide	$C_5H_5N_3O$	123.11
20	5-(Hydroxymethyl)-2-furaldehyde (HMF)	$C_6H_6O_3$	126.11
21	Flucytosine	$C_4H_4FN_3O$	129.09
22	Agmatine	$C_5H_{14}N_4$	130.19
23	Leucine	$C_6H_{13}NO_2$	131.17
24	Paraldehyde	$C_6H_{12}O_3$	132.16
25	5-amino-1,3,4-thiadiazole-2-thiol	$C_2H_3N_3S_2$	133.2
26	Timonacic	$C_4H_7NO_2S$	133.17
27	Fluciclovine	$C_5H_8FNO_2$	133.12
28	Tranylcypromine	$C_9H_{11}N$	133.19
29	Malic acid	$C_4H_6O_5$	134.09
30	Amphetamine	$C_9H_{13}N$	135.21
31	Eniluracil	$C_6H_4N_2O_2$	136.11
32	Betahistine	$C_8H_{12}N_2$	136.19
33	Isoniazid	$C_6H_7N_3O$	137.14
34	Tramiprosate	$C_3H_9NO_3S$	139.18
35	Dimiracetam	$C_6H_8N_2O_2$	140.14
36	Coenzyme M	$C_2H_6O_3S_2$	142.2
37	Piracetam	$C_6H_{10}N_2O_2$	142.16
38	4-isothioureidobutyronitrile	$C_5H_9N_3S$	143.21
39	Valnoctamide	$C_8H_{17}NO$	143.23
40	Dimethyl fumarate	$C_6H_8O_4$	144.12

3.3. Predictions of E_b with neural networks

Neural networks are suitable tools for recognizing of complex non-linear dependencies. It would be very attractive to predict binding energy between fullerenes and drug based on drug properties only, especially for extensive consideration of large sets of drugs. According to the conceptual density functional theory, the frontier orbitals and the dipole moment determine the chemical reactivity of the drug and therefore may hypothetically be relevant for its interaction with fullerene. Therefore, we constructed artificial neural networks to predict the E_b based on HOMO, LUMO and D of the loaded drug.

For each fullerene, 1000 networks were constructed and learnt. All networks had three input (for HOMO, LUMO and D of the drug) and single output (for E_b) neurons, interacting via a single hidden layer. Other parameters were randomly distributed in the following ranges: number of neurons in hidden layer – 3 to 10; activation functions – identical, hyperbolic tangential, exponential, hyperbolic, logistic. For learning of networks, all data were randomly divided into three sets: training (70%), testing (15%) and validation (15%). Learning was carried out with the BFGS algorithm. Sum of squares (SOS) error function was applied. The parameters and productivities of the best networks are summarized in Table 5. This table shows mean absolute errors of E_b value lower than 0.1 eV, whereas maximal errors are substantially higher. Therefore, the presented networks provide only a quite rough estimation of E_b and have a limited applicability.

3.4. Exceptionally strong adsorption of altretamine drug on fullerenes

Among all considered molecules, we recognized altretamine, a drug used for ovarian cancer treatment. It possesses the highest E_b values for all considered fullerenes, which deviate from mean values by about 3σ. According to Supplementary materials Table S5, this result is also confirmed by calculations with four different exchange–correlation functionals. The structure of altretamine is shown in Fig. 2(a), and its adsorption on fullerenes are shown in Fig. 2 (b-d).

Table 2
The minimum, maximum and mean values of adsorption energy E_b and deformation energies E_{def}(full) and E_{def}(drug) calculated for 40 drugs adsorbed on C_{60}, $C_{60}F_2$ and $C_{60}F_{48}$ fullerenes. Standard deviations σ are also presented.

	E_b, eV				E_{def}(full), meV				E_{def}(drug), meV			
	min	max	mean	σ	min	max	mean	σ	min	max	mean	σ
C_{60}	0.098	0.75	0.41	0.10	0.00	17.92	8.64	3.60	1.85	204.37	35.20	48.06
$C_{60}F_2$	0.28	0.98	0.59	0.14	2.25	33.83	12.03	6.50	4.17	343.15	57.90	67.24
$C_{60}F_{48}$	0.39	0.87	0.54	0.09	2.04	117.9	16.57	20.54	0.00	174.99	26.55	34.77

Table 3
Pair correlations coefficients for the values of the binding energy E_b, deformation energies E_{def}(full) and E_{def}(drug), as well as frontier orbitals HOMO and LUMO and dipole moments D of the pristine and loaded drugs. Correlation coefficients larger that 0.500 were marked in bold.

	E_{def} (full)	E_{def} (drug)	HOMO (drug)	HOMO (full + drug)	LUMO (drug)	LUMO (full + drug)	D (drug)	D (full + drug)	E_b
Pristine C_{60}									
E_{def} (full)	1.000	−0.432	−0.133	−0.013	−0.006	0.154	−0.233	−0.294	−0.298
E_{def} (drug)	−0.432	1.000	−0.112	−0.192	−0.150	−0.258	-0.132	0.319	0.340
HOMO (drug)	−0.133	−0.112	1.000	**0.753**	0.333	0.354	0.131	−0.001	0.350
HOMO (full + drug)	−0.013	−0.192	0.753	1.000	0.208	**0.708**	−0.023	−0.242	0.280
LUMO (drug)	−0.006	−0.150	0.333	0.208	1.000	0.132	−0.162	−0.080	−0.240
LUMO (full + drug)	0.154	−0.258	0.354	0.708	0.132	1.000	−0.103	−0.480	0.130
D (drug)	−0.233	0.132	0.131	−0.023	−0.162	−0.103	1.000	**0.708**	0.110
D (full + drug)	−0.294	0.319	−0.001	−0.242	−0.080	−0.480	0.780	1.000	0.110
E_b	−0.298	0.341	0.354	0.282	−0.243	0.139	0.118	0.118	1.000
$C_{60}F_2$									
E_{def} (full)	1.000	0.179	−0.034	−0.111	−0.026	0.142	0.222	0.365	0.251
E_{def} (drug)	0.179	1.000	−0.002	0.083	−0.130	0.003	0.232	0.207	−0.258
HOMO (drug)	−0.034	−0.002	1.000	**0.828**	0.333	0.104	0.131	0.080	0.289
HOMO (full + drug)	−0.111	0.083	0.828	1.000	0.199	0.210	0.055	0.020	0.272
LUMO (drug)	−0.026	−0.130	0.333	0.199	1.000	0.063	−0.162	−0.197	−0.135
LUMO (full + drug)	0.142	0.003	0.104	0.210	0.063	1.000	0.050	−0.069	0.078
D (drug)	0.222	0.232	0.131	0.055	−0.162	0.050	1.000	**0.932**	0.154
D (full + drug)	0.365	0.207	0.080	0.020	−0.197	−0.069	0.932	1.000	0.292
E_b	0.251	−0.258	0.289	0.272	−0.135	0.078	0.154	0.292	1.000
$C_{60}F_{48}$									
E_{def} (full)	1.000	0.290	0.139	0.081	−0.245	0.500	0.246	0.261	0.187
E_{def} (drug)	0.290	1.000	0.384	0.431	0.007	0.002	0.030	0.089	0.105
HOMO (drug)	0.139	0.384	1.000	**0.972**	0.333	−0.004	0.131	0.080	0.190
HOMO (full + drug)	0.081	0.431	0.972	1.000	0.326	−0.165	0.164	0.138	0.153
LUMO (drug)	−0.245	0.007	0.333	0.326	1.000	−0.046	−0.162	−0.197	−0.145
LUMO (full + drug)	0.500	0.002	−0.004	−0.165	−0.046	1.000	−0.130	−0.269	0.087
D (drug)	0.246	0.030	0.131	0.164	−0.162	−0.130	1.000	**0.932**	−0.017
D (full + drug)	0.261	0.089	0.080	0.138	−0.197	−0.269	0.932	1.000	0.036
E_b	0.187	0.105	0.190	0.153	−0.145	0.087	−0.017	0.036	1.000

Table 4
Multiple coefficients of determination R^2 for multiple linear regressions of binding energies between fullerenes and drugs E_b as a function of eight other values listed in Table 3. Maximal, minimal and mean absolute differences (eV) between actual and predicted from regressions values of E_b are also presented.

	R^2	absolute deviations of E_b		
		min	max	mean
C_{60}	0.43	0.001	0.274	0.043
$C_{60}F_2$	0.46	0.001	0.329	0.078
$C_{60}F_{48}$	0.15	0.000	0.300	0.068

Table 5
Parameters of the best obtained neural networks for prediction of adsorption energy of drugs on pristine and fluorinated fullerenes based on drug HOMO, LUMO and dipole moment. Learning algorithms, activation functions of hidden and output neurons (logistic, exponential or hyperbolic) and absolute deviations of predicted E_b from its actual value (eV) are presented. Number of neurons in input, hidden and output layers and number of iterations of Broyden–Fletcher–Goldfarb–Shanno (BFGS) algorithm needed for convergence are indicated in second and third columns, respectively.

system	network name	learning algoruthm	activation (hidden)	activation (output)	absolute deviations of E_b		
					min	max	mean
C_{60}	MLP-3–3-1	BFGS-43	LOGISTIC	EXP	0.000	0.143	0.043
$C_{60}F_2$	MLP-3–4-1	BFGS-32	HYPER	HYPER	0.001	0.227	0.089
$C_{60}F_{48}$	MLP-3–9-1	BFGS-1	EXP	EXP	0.000	0.323	0.068

The molecule has almost flat skeleton consisted of alternating C and N atoms, terminated by methyl groups. It is located parallel to fullerene surface, allowing interaction between fullerene rings and drug heterocycle. Curvature of pristine fullerene provides sufficient distance between fullerene and methyl groups, which do not prevent fullerene-drug interaction. Low fluorination of fullerene provides additional interaction of methyl groups with fluorine. High fluorinated fullerenes imply attraction of fluorine to nitrogen atoms. Previously, BN and AlN nanorings [36] as well as cucurbit[n]uril [37] were considered for delivery of altretamine. However, interaction of this drug with fullerenes or other carbon-based carriers was not investigated so far. To facilitate the spectroscopic control of the loading process, we calculated infrared spectral shifts associated with the adsorption. The results are presented in Fig. 3. As one can see from Fig. 3, small red shifts near 1450 cm^{-1} corresponding to methyl groups deformation vibrations can be selected as the suitable indicator of the drug loading.

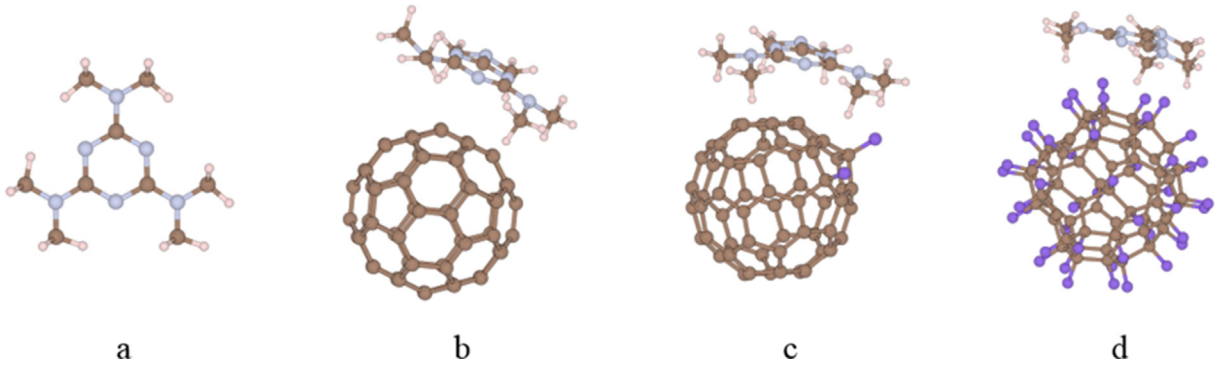

Fig. 2. The structure of altretamine drug (a) and its adsorption on fullerenes C_{60} (b), $C_{60}F_2$ (c) and $C_{60}F_{48}$ (d). Fullerenes in Fig. 2b, 2c and 2d corresponds to fulleneres showns in Fig. 1a, 1b and 1c, respectively. The brown and purple balls represent carbon and fluorine atoms, respectively. Drug consist also nitrogen and hydrogen atoms, which are represented by blue and grey balls, respectively. (For interpretation of the references to colour in this figure legend, the reader is referred to the web version of this article.)

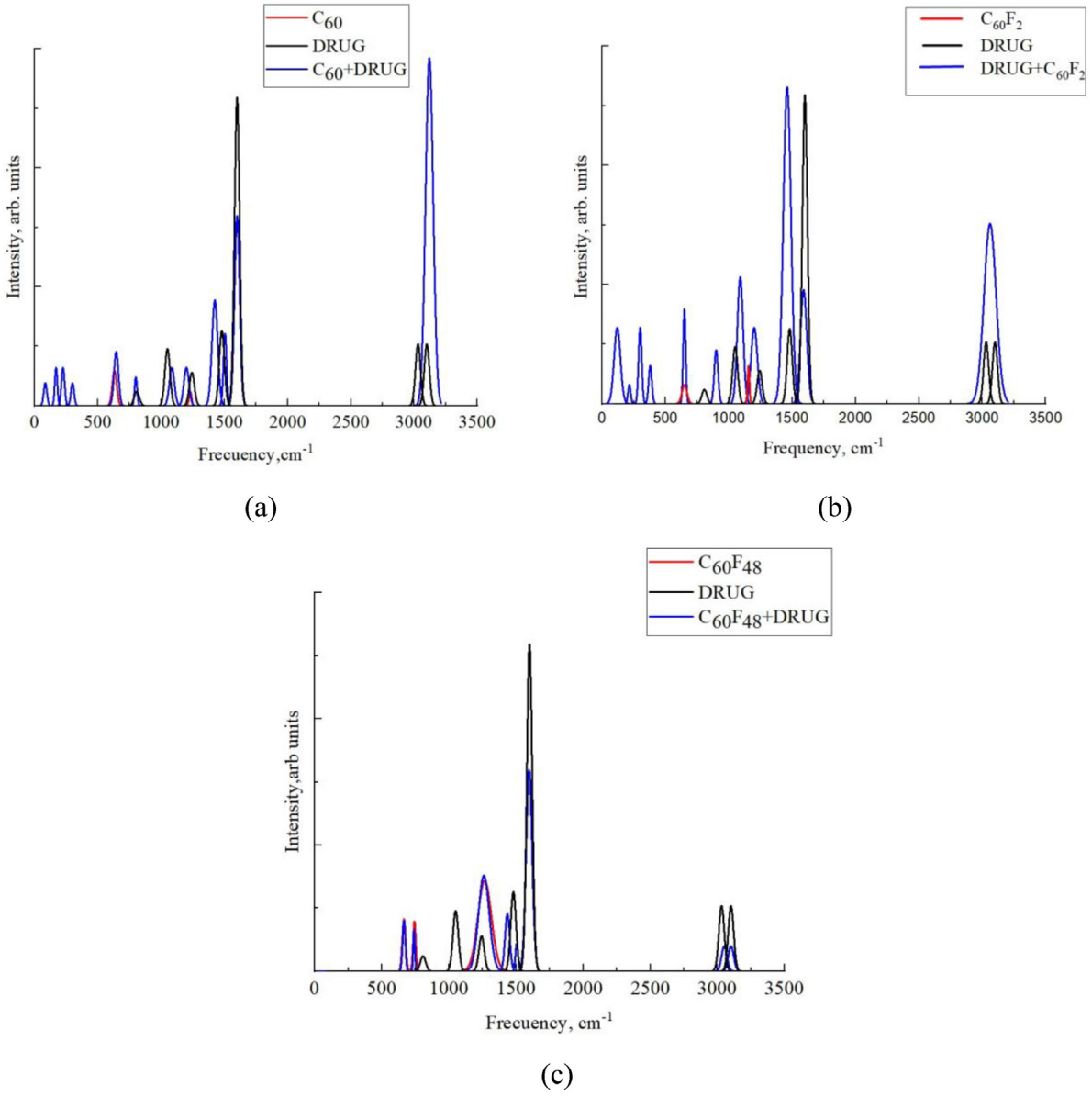

Fig. 3. Infrared active modes calculated for pristine and loaded on C_{60} (a), $C_{60}F_2$ (b) and $C_{60}F_{48}$ (c) altretamine drug. The calculated active frequencies are broadened by Gaussians with σ = 20 cm^{-1}.

4. Conclusion

In summary, we provided a systematic study of the interaction between pristine and fluorinated fullerenes with a set of 40 low molecular weight drugs. We have established the range to which the binding energy between fullerene and drugs belongs, as well as the shift of the boundaries of this range due to fluorination. Mean adsorption energies of drugs on C_{60}, $C_{60}F_2$ and $C_{60}F_{48}$ are 0.41, 0.59 and 0.54 eV, respectively, whereas standard deviations σ are about 0.1 eV for all cases. The presented data can be used as a reference point for evaluating the reactivity and selectivity of pristine or fluorinated fullerenes toward any new molecule. The excess of the adsorption energy over the average value by 2σ (0.2 eV) and 3σ (0.3 eV) should be considered as an indicator of a strong and exceptionally strong drug-fullerene interactions, respectively. In particular, we observed exceptionally strong binding of fullerenes with the altretamine molecule containing a hexagonal $(CN)_3$ heterocycle (E_b = 0.75, 0.98 and 0.87 eV for C_{60}, $C_{60}F_2$ and $C_{60}F_{48}$ fullerenes, respectively). One can also expect strong interaction between fullerenes and similar molecules with nitro-carbon skeletons, such as dactinomycin (anticancer drug) or enzalutamide (antineoplastic hormonal agent).

In addition, we evaluated the accuracy of the adsorption energies of drugs on fullerenes predicted based on statistical data and commonly used quantum chemical descriptors of reactivity. According to our calculations, an accurate prediction is impossible, and the typical absolute value of the error is about 0.1 eV. However, even such low accuracy can be useful for primary selection for the computational study of extensive sets of drugs. We believe that the presented results are useful for understanding the interaction of fluorinated fullerenes with drugs and for reasonable design of suitable drugs delivery systems.

CRediT authorship contribution statement

Elizaveta B. Kalika: Software, Validation, Formal analysis, Investigation, Resources, Data curation, Visualization. **Nikolay V. Bondarev:** Methodology, Software, Validation, Formal analysis, Data curation. **Konstantin P. Katin:** Conceptualization, Methodology, Software, Validation, Formal analysis, Investigation, Writing – original draft, Project administration, Funding acquisition. **Alexey I. Kochaev:** Conceptualization, Methodology, Data curation, Writing – review & editing, Visualization, Supervision. **Anastasiya A. Grekova:** Software, Validation, Formal analysis, Investigation. **Savas Kaya:** Software, Validation, Formal analysis, Investigation. **Yusupbek A. Bauetdinov:** Formal analysis, Investigation, Data curation. **Mikhail M. Maslov:** Conceptualization, Methodology, Writing – original draft, Visualization, Supervision.

Data availability

Data are available as a supplementary materials.

Declaration of Competing Interest

The authors declare that they have no known competing financial interests or personal relationships that could have appeared to influence the work reported in this paper.

Acknowledgements

Russian Science Foundation (project 20-73-00245) financially supported the reported study. Konstantin Katin and Mikhail Maslov are grateful to the MEPhI program Priority 2030. A fragment of graphical abstract (drugs images) was designed by sentavio / Freepik.

Appendix A. Supplementary material

Supplementary data to this article can be found online at https://doi.org/10.1016/j.molliq.2023.121559.

References

[1] F. Moussa. Fullerene and derivatives for biomedical applications. Nanobiomaterials: Nanostructured Materials for Biomedical Applications. Chapter 5: [60]Fullerene and derivatives for biomedical applications. Elsevier, 2018, 113-136. https://doi.org/10.1016/B978-0-08-100716-7.00005-2.

[2] Y. Prylutskyy, O. Matyshevska, S. Prylutska, A. Grebinyk, M. Evstigneev, S. Grebinyk, L. Skivka, V. Cherepanov, A. Senenko, R. Stoika, U. Ritter, P. Scharff, T. Dandekar, M. Frohme, A Novel Water-Soluble C60 Fullerene-Based Nano-Platform Enhances Efficiency of Anticancer Chemotherapy, Biomed. Nanomater. (2021) 59–93, https://doi.org/10.1007/978-3-030-76235-3_3.

[3] İ. Muz, F. Göktaş, M. Kurban, A density functional theory study on favipiravir drug interaction with BN-doped C60 heterofullerene, Physica E 135 (2022) 114950.https://doi.org/10.1016/j.physe.2021.114950.

[4] M.D. Esrafili, A.A. Khan, Alkali metal decorated C60 fullerenes as promising materials for delivery of the 5-fluorouracil anticancer drug: a DFT approach, RSC Adv. 12 (2022) 3948–3956, https://doi.org/10.1039/d1ra09153k.

[5] D. Fouejio, R.A. Yossa Kamsi, Y. Tadjouteu Assatse, G.W. Ejuh, J.M.B. Ndjaka, DFT studies of the structural, chemical descriptors and nonlinear optical properties of the drug dihydroartemisinin functionalized on C_{60} fullerene, Comput. Theor. Chem. 1202 (2021) 113298. https://doi.org/10.1016/j.comptc.2021.113298.

[6] C. Parlak, Ö. Alver, Ö. Bağlayan, Quantum mechanical simulation of Molnupiravir drug interaction with Si-doped C_{60} fullerene, Comput. Theor. Chem. 1202 (2021), https://doi.org/10.1016/j.comptc.2021.113336.

[7] P. Wang, G. Yan, X. Zhu, Y. Du, D. Chen, J. Zhang, Heterofullerene MC59 (M = B, Si, Al) as Potential Carriers for Hydroxyurea Drug Delivery, Nanomaterials 11 (2021) 115, https://doi.org/10.3390/nano11010115.

[8] R. Neal, P.N. Samanta, J. Leszczynski, First-principles modeling of complexation of anticancer antibiotics with fullerene (C60) nanocage: Probing non-covalent interactions by vibrational and electronic spectroscopy, J. Mol. Struct. 1255 (2022), https://doi.org/10.1016/j.molstruc.2022.132449.

[9] M. Nouraliei, H. Javadian, K. Mehdizadeh, N. Sheibanian, A.S. Douk, F. Mohammadzadeh, N. Osouleddini, Fullerene carbon nanostructures for the delivery of phenelzine derivatives as new drugs to inhibit monoamine oxidase enzyme: Molecular docking interactions and density functional theory calculations, Colloids Surf. A 657 (2023) 130599.https://doi.org/10.1016/j.colsurfa.2022.130599.

[10] S. Wu, L. Lu, L. Li, Q. Liang, H. Gao, X. Zhao, D. Hu, T. Tang, Y. Tang, Density Functional Study of the adsorption behavior of 6-mercaptopurine on Primary, Si, Al and Ti doped C_{60} fullerenes, Chem. Phys. Lett. 804 (2022) 139910. https://doi.org/10.1016/j.cplett.2022.139910.

[11] Z. Hadi, M. Nouraliei, A. Yousefi-Siavoshani, H. Javadian, S.M. Chalanchi, S.S. Hashemi, A DFT study on the therapeutic potential of carbon nanostructures as sensors and drug delivery carriers for curcumin molecule: NBO and QTAIM analyses, Colloids Surf. A 651 (2022), https://doi.org/10.1016/j.colsurfa.2022.129698.

[12] M. Govindappa, A. Vishaka, B.S. Akshatha, D. Popli, N. Sunayana, C. Srinivas, A. Pugazhendhi, V.B. Raghavendra, An endophytic fungus, Penicillium simplicissimum conjugated with C60 fullerene for its potential antimitotic, anti-inflammatory, anticancer and photodegradation activities, Envir. Tech. (2021) 1–15.https://doi.org/10.1080/09593330.2021.1985621.

[13] İ. Muz, Enhanced adsorption of fluoroquinolone antibiotic on the surface of the Mg-, Ca-, Fe- and Zn-doped C_{60} fullerenes: DFT and TD-DFT approach, Mater. Today Comm. 31 (2022), https://doi.org/10.1016/j.mtcomm.2022.103798.

[14] İ. Muz, M. Kurban, A first-principles evaluation on the interaction of 1,3,4-oxadiazole with pristine and B-, Al-, Ga-doped C_{60} fullerenes, J. Mol. Liquids 335 (2021), https://doi.org/10.1016/j.molliq.2021.116181.

[15] E. Alipour, S. Maleki, N. Razavipour, N. Hajali, S. Jahani, Identification of amphetamine as a stimulant drug by pristine and doped C_{70} fullerenes: a DFT/TDDFT investigation, J. Mol. Model. 27 (2021) 169, https://doi.org/10.1007/s00894-021-04788-z.

[16] P. Gong, L. Zhang, X. Yuan, X. Liu, X. Diao, Q. Zhao, Z. Tian, J. Sun, Z. Liu, J. You, Multifunctional fluorescent PEGylated fluorinated graphene for targeted drug delivery: An experiment and DFT study, Dyes and Pigments 162 (2019) 573–582.https://doi.org/10.1016/j.dyepig.2018.10.031.

[17] P. Gong, S. Ji, J. Wang, D. Dai, F. Wang, M. Tian, L. Zhang, F. Guo, Z. Liu, Fluorescence-switchable ultrasmall fluorinated graphene oxide with high near-infrared absorption for controlled and targeted drug delivery, Chem. Eng. J. 348 (2018) 438–446, https://doi.org/10.1016/j.cej.2018.04.193.

[18] M. Jahanshahi, E. Kowsari, V. Haddadi-Asl, M. Khoobi, B. Bazri, M. Aryafard, J.H. Lee, F.B. Kadumudi, S. Talebian, N. Kamaly, M. Mehrali, A. Dolatshahi-Pirouz,

An innovative and eco-friendly modality for synthesis of highly fluorinated graphene by an acidic ionic liquid: Making of an efficacious vehicle for anti-cancer drug delivery, Appl. Surf. Sci. 515 (2020), https://doi.org/10.1016/j.apsusc.2020.146071.

[19] M. Razaghi, A. Ramazani, M. Khoobi, T. Mortezazadeh, E.A. Aksoy, T.T. Küçükkılınç, Highly fluorinated graphene oxide nanosheets for anticancer linoleic-curcumin conjugate delivery and T2-Weighted magnetic resonance imaging: In vitro and in vivo studies, J. Drug Delivery Sci. Tech. 60 (2020), https://doi.org/10.1016/j.jddst.2020.101967.

[20] P. Gong, J. Du, D. Wang, B. Cao, M. Tian, Y. Wang, L. Sun, S. Ji, Z. Liu, Fluorinated graphene as an anticancer nanocarrier: an experimental and DFT study, J. Mater. Chem. B 6 (2018) 2769–2777, https://doi.org/10.1039/c8tb00102b.

[21] D. Wang, Y. Zhang, M. Zhai, Y. Huang, H. Li, X. Liu, P. Gong, Z. Liu, J. You, Fluorescence Turn-off Magnetic Fluorinated Graphene Composite with High NIR Absorption for Targeted Drug Delivery, ChemNanoMat 7 (2020) 71–77, https://doi.org/10.1002/cnma.202000539.

[22] P. Gong, F. Wang, F. Guo, J. Liu, B. Wang, X. Ge, S. Li, J. You, Z. Liu, Fluorescence turn-off Ag/fluorinated graphene composites with high NIR absorption for effective killing of cancer cells and bacteria, J. Mater. Chem. B 6 (2018) 7926–7935, https://doi.org/10.1039/c8tb02211a.

[23] E.B. Kalika, K.P. Katin, A.I. Kochaev, S. Kaya, M. Elik, M.M. Maslov, Fluorinated carbon and boron nitride fullerenes for drug Delivery: Computational study of structure and adsorption, J. Mol. Liquids 353 (2022), https://doi.org/10.1016/j.molliq.2022.118773.

[24] V.S. Prudkovskiy, K.P. Katin, M.M. Maslov, P. Puech, R. Yakimova, G. Deligeorgis, Efficient cleaning of graphene from residual lithographic polymers by ozone treatment, Carbon 109 (2016) 221–226, https://doi.org/10.1016/j.carbon.2016.08.013.

[25] K.P. Katin, A.I. Kochaev, S. Kaya, F. El-Hajjaji, M.M. Maslov, Ab Initio Insight into the Interaction of Metal-Decorated Fluorinated Carbon Fullerenes with Anti-COVID Drugs, IJMS 23 (2022) 2345, https://doi.org/10.3390/ijms23042345.

[26] S. Seritan, C. Bannwarth, B.S. Fales, E.G. Hohenstein, S.I.L. Kokkila-Schumacher, N. Luehr, J.W. Snyder Jr., C. Song, A.V. Titov, I.S. Ufimtsev, T.J. Martínez, TeraChem: Accelerating electronic structure and ab initio molecular dynamics with graphical processing units, J. Chem. Phys. 152 (2020), https://doi.org/10.1063/5.0007615.

[27] L.-P. Wang, C. Song, Geometry optimization made simple with translation and rotation coordinates, J. Chem. Phys. 144 (2016), https://doi.org/10.1063/1.4952956.

[28] A.D. Becke, Density-functional thermochemistry. III. The role of exact exchange, J. Chem. Phys. 98 (2019) 5648–5652.

[29] C. Lee, W. Yang, R.G. Parr, Development of the Colle-Salvetti correlation-energy formula into a functional of the electron density, Phys. Rev. B 37 (1988) 785–789, https://doi.org/10.1103/PhysRevB.37.785.

[30] M. Tanaka, M. Katouda, S. Nagase, Optimization of RI-MP2 Auxiliary Basis Functions for 6–31G** and 6–311G** Basis Sets for First-, Second-, and Third-Row Elements, J. Comput. Chem. 34 (2013) 2568–2575, https://doi.org/10.1002/jcc.23430.

[31] S. Grimme, J. Antony, S. Ehrlich, H. Krieg, A consistent and accurate ab initio parametrization of density functional dispersion correction (DFT-D) for the 94 elements H-Pu, J. Chem. Phys. 132 (2010), https://doi.org/10.1063/1.3382344.

[32] N.V. Bondarev, Computer Analysis of Stability of Alkaline Metal Cation M[222] + Cryptates in Different Solvents, Russ. J. Gen. Chem. 91 (2021) 409–428, https://doi.org/10.1134/S1070363221030117.

[33] Statsoft. http://statsoft.ru/products/STATISTICA_Neural_Networks (accessed: October 2022).

[34] K. Momma, F. Izumi, Vesta 3 for three-dimensional visualization of crystal, volumetric and morphology data, J. Appl. Cryst. 44 (2011) 1272–1276, https://doi.org/10.1107/S0021889811038970.

[35] D.S. Wishart, C. Knox, A.C. Guo, S. Shrivastava, M. Hassanali, P. Stothard, Z. Chang, J. Woolsey, DrugBank: a comprehensive resource for in silico drug discovery and exploration, Nucl. Acids Res. 34 (2006) D668–D672, https://doi.org/10.1093/nar/gkj067.

[36] M. Khaleghian, F. Azarakhshi, Theoretical modelling of encapsulation of the Altretamine drug into $BN_{(9,9-5)}$ and $AlN_{(9,9-5)}$ nano rings: a DFT study, Mol. Phys. 117 (2019) 2559–2569, https://doi.org/10.1080/00268976.2019.1574987.

[37] K. Hassanzadeh, K. Akhtari, S.S. Esmaeili, A. Vaziri, H. Zamani, M. Maghsoodi, S. Noori, A. Moradi, P. Hamidi, Encapsulation of Thiotepa and Altretamine as neurotoxic anticancer drugs in Cucurbit[n]uril (n=7, 8) nanocapsules: A DFT study, J. Theor. Comput. Chem. 15 (2016) 1650056, https://doi.org/10.1142/s0219633616500565.